

Chiral Superconductivity in Thin Films of Bi_2Se_3

Luca Chirrolli¹

¹IMDEA-Nanoscience, Calle de Faraday 9, E-28049 Madrid, Spain*

Recent experimental evidences point to rotation symmetry breaking superconductivity in doped Bi_2Se_3 , where the relevant order parameter belongs to a two-component odd-parity representation E_u of the crystal point group. The E_u channel admits two possible phases, the chiral phase, that breaks time-reversal symmetry, and nematic phase, that well explains the reported rotation symmetry breaking. In weakly anisotropic three-dimensional systems the nematic phase is the stable one. We study the stability of the nematic phase versus the chiral phase as a function of the anisotropy of the system and the thickness of the sample and show that in the strongly anisotropic case or in thin slabs the chiral phases is favoured. For the extreme 2D limit composed by a single layer of Bi_2Se_3 the system hosts two chiral Majorana modes flowing at the boundary of the system.

PACS numbers: 74.20.Rp, 74.20.Mn, 74.90.+n

I. INTRODUCTION

Chiral superconductivity is a topological quantum state of matter in which an unconventional superconductor spontaneously breaks time-reversal symmetry and develops an intrinsic angular momentum¹. Its peculiar gap structure usually favours a single spin component and induces a $p_x + ip_y$ state that is topologically non-trivial. Key signatures in two-dimensional (2D) systems are surfaces chiral Majorana modes and Majorana zero energy states in vortex cores^{2–7}. In three dimensions, chiral superconductivity (SC) is also possible, allowing the realization of a Weyl superconductor with Majorana arcs on the surface^{8–10}, but realistic candidate materials for this superconducting state are lacking. Chiral superconductors have attracted great interest for their unconventional character and their potential use in the field of quantum computation^{11,12}.

Recently, strong experimental evidences of unconventional superconductivity have been reported for a well known material, Bi_2Se_3 , that in its pristine form is a Topological Insulator (TI)^{13,14}. The first studies were originally motivated by the prediction of three dimensional, time-reversal invariant (TRI) topological superconductivity in centrosymmetric systems¹⁵. Possibly odd-parity superconductivity was first reported in Bi_2Se_3 intercalated with Cu^{16–18}, although clear evidence for the characteristic surface Andreev states has remained controversial^{19–21}. A much richer phenomenology has recently emerged, showing a broken C_3 symmetry in the superconducting state in samples intercalated with Cu, Nb, and Sr^{22–25}. Several experiments reported uniaxial anisotropy response to an in-plane magnetic field in the Knight shift²⁶, the upper critical field^{27,28}, the magnetic torque²⁵, and the specific heat²⁷. Specific heat¹⁸ and penetration depth^{29,30} have excluded the presence of line nodes on the Fermi surface. All these observations support a pairing state of nematic type belonging to the two-component representation E_u of the crystal point group^{31,32}.

Theoretical modelling have also discussed different as-

pects of the E_u states, covering from bulk properties^{33–35}, to surface states³⁶, vortex states^{37,38}, the interplay between E_u superconductivity and magnetism in promoting time-reversal symmetry breaking states^{39,40}, and the role of odd-parity fluctuations as the mechanism at the basis of E_u superconductivity⁴¹ and preemptive nematicity above T_c ⁴².

In this work we study superconductivity in Bi_2Se_3 in the E_u odd-parity channel, focusing on the stability of the nematic phase versus the chiral phase as a function of the anisotropy of the system and the thickness of the sample. Bi_2Se_3 is a layered material in which the unit cell is constituted by a quintuple layer structure. It is therefore reasonable to study the behaviour of the system by varying the interlayer coupling and the chemical potential. We show that an increase of the anisotropy along the out-of-plane direction favours the chiral phase. Chemical dopants intercalate between the unit cells and modify their distance and relative coupling, together with the charge density. Strong anisotropy can be achieved by increasing the doping or by properly choosing the dopants so to increase the interlayer spacing of the materials.

Interestingly, a second root towards chiral superconductivity is provided by exfoliation. In particular, the chiral phase is the natural phase of the E_u channel in the extreme 2D limit of a single layer^{31,32}. We show that by reducing the thickness of the sample without increasing the anisotropy of the systems naturally drives the system towards the chiral phase. We find as rough estimates that a thin slabs with approximately ten layers marks the stability threshold between the nematic and the chiral phase. Experimentally, exfoliation down to the single QL case has been achieved^{43,44}, so that this root shows a promising way to obtain chiral quasi-2D superconductors.

The low energy Hamiltonian of the system is a massive Dirac Hamiltonian, so that our results apply to generic systems that share the same low energy description, such as Rashba bilayer system⁴⁵.

The topological character of the 2D system is inherited from the 3D bulk topological charge $C = \pm 2$ Weyl points that arise on the Fermi surface in the chiral phase^{32,39}.

Starting from a tight-binding model that well approximates the complicated band structure of Bi_2Se_3 , we show that the chiral phase in this material supports $C = 2$ chiral Majorana modes that co-propagate at the boundary of the system and can find useful applications in interferometric schemes⁴⁶.

The work is structured as follows: in Sec. II we review the known analysis of the two-component superconducting channel of the D_{3d} crystal point group. In Sec. III we derive the Ginzburg Landau function that describes the condensation of the two-component channel. In Sec. IV we study the stability of the chiral phase and show that in the strong anisotropic case it is the favoured phase. In Sec. V we show that by reducing the thickness of the sample a chiral phase is obtained for thin slabs. In Sec. VI we study the surface states through a tight-binding numerical simulation. Finally, in Sec. VII we conclude with a summary of the results.

II. E_u SUPERCONDUCTIVITY

We consider doped Bi_2Se_3 in the $k \cdot p$ low energy approximation introduced in Ref. [15]. The point group of the crystal is D_{3d} and system can be described by a simplified model in which the unit cell is constituted by a bilayer structure where spin s electrons occupy p_z -like orbitals on the top (T) and bottom (B) layers. The low energy Hamiltonian then reads

$$H_{\mathbf{k}}^0 = m\sigma_x + v(k_x s_y - k_y s_x)\sigma_z + v_z k_z \sigma_y, \quad (1)$$

where Pauli matrices σ_i and s_i describe the orbital and spin degrees of freedom, respectively. The Hamiltonian is TRI, where the time reversal operator is $\mathcal{T} = is_y K$ with K complex conjugation and commutes with H_0 .

Superconductivity is described within the Bogoliubov deGennes (BdG) formalism by introducing the Nambu spinor $\Psi_{\mathbf{k}} = (\mathbf{c}_{\mathbf{k}}, is_y \mathbf{c}_{-\mathbf{k}}^\dagger)^T$, with $\mathbf{c}_{\mathbf{k}}$ fermionic annihilation operators of the band insulator Hamiltonian $H_{\mathbf{k}}^0$. The Hamiltonian reads $\hat{\mathcal{H}} = \frac{1}{2} \int d\mathbf{k} \Psi_{\mathbf{k}}^\dagger H(\mathbf{k}) \Psi_{\mathbf{k}}$, with

$$H_{\mathbf{k}} = (H_{\mathbf{k}}^0 - \mu)\tau_z + \Delta_{\mathbf{k}}\tau_+ + \Delta_{\mathbf{k}}^\dagger\tau_-, \quad (2)$$

and with $\Delta_{\mathbf{k}}$ generic momentum-dependent 4×4 gap matrices. The Nambu construction imposes that $H_{\mathbf{k}}$ has a charge conjugation symmetry C implemented as $U_C H(-\mathbf{k})^* U_C^\dagger = -H(\mathbf{k})$, with $U_C = s_y \tau_y$. C imposes a restriction on the pairing matrix, $s_y \Delta^*(-\mathbf{k}) s_y = \Delta(\mathbf{k})$. If pairing is momentum independent, there are only 6 possible matrices in the irreducible representations of the D_{3d} point group that satisfy this constraint and they have been classified in Ref. [15]. Accordingly, they are given by the even parity channel I and σ_x belonging to the A_{1g} , and the odd-parity channel $\sigma_y s_z$ belonging to A_{1u} , σ_z belonging to A_{2u} , and $(-\sigma_y s_y, \sigma_y s_x)$ belonging to E_u . In particular, the latter forms a two-component representation that can describe nematic SC^{31,32}.

Focusing on the E_u odd-parity channel we associate to the matrix operators the following order parameters

$$\psi = (\psi_x, \psi_y) \sim (-\sigma_y s_y, \sigma_y s_x) \sim E_u.$$

In Ref. [15] it was shown that when only local pairing interaction is considered, the A_{1u} is the leading instabilities in a wide range of parameters in the phase diagram. On the other hand, the author has shown that inclusion of momentum-dependent pairing interaction terms only affects the critical temperature of the nematic channel E_u ³⁹, rising it with respect to the critical temperature of the A_{1u} channel. Recently, odd-parity fluctuations together with repulsive Coulomb interactions have also emerged as a possible mechanism that selects the E_u odd-parity two-component channel as the leading SC channel⁴¹. We then assume that the nematic channel condenses and focus on the competition between the nematic and chiral phases.

III. GINZBURG LANDAU THEORY

We start considering the vector phase ψ and study the conditions under which a chiral phase occurs. Symmetry dictates the form of its free energy that reads

$$F_\psi = a|\psi|^2 + b_1|\psi|^4 + b_2|\psi_x \psi_y^* - \psi_y \psi_x^*|^2. \quad (3)$$

The E_u representation admits two possible superconducting states: a nematic state $\psi \propto (1, 0)$ which is time-reversal invariant and has point nodes on the equator of the Fermi surface, and a chiral state $\psi \propto (1, i)$ which breaks TR symmetry and has $C = \pm 2$ Weyl nodes at the north and south pole of the Fermi surface³². The sign of the coupling b_2 determines whether the vector representation chooses the nematic (for $b_2 > 0$) or the chiral state (for $b_2 < 0$). Microscopic calculations show that for a 3D isotropic model $b_2 > 0$, so that no TRB phase may arise in the system^{31,32}. We now specifically study the sign of the coupling b_2 versus anisotropy and sample thickness.

Setting the chemical potential in the conduction band, $\mu > m$, we can reduce the dimensionality of the problem by projecting the Hamiltonian and the gap matrix down to the conduction band, so that the gap matrix reads

$$\Delta_{\mathbf{k}} = \psi_x \mathbf{d}_x \cdot \tilde{\mathbf{s}} + \psi_y \mathbf{d}_y \cdot \tilde{\mathbf{s}}, \quad (4)$$

where $\mathbf{d}_x = (0, -\tilde{k}_z, \tilde{k}_y)$ and $\mathbf{d}_y = (\tilde{k}_z, 0, -\tilde{k}_x)$, the momentum has been rescaled as $\tilde{\mathbf{k}} = (v k_x, v k_y, v_z k_z) / \mu$, and $\tilde{\mathbf{s}}$ is a momentum-dependent spin-1/2 like vector operator parametrizing the twofold degenerate subspace at every \mathbf{k} point associated to Kramers degeneracy⁴⁷. Explicitly, defining $|\psi_{\mathbf{k},1}\rangle$ and $|\psi_{\mathbf{k},2}\rangle$ the two degenerate eigenstates in the conduction band at momentum \mathbf{k} , the vector $\tilde{\mathbf{s}}$ is obtained as $\tilde{s}_x = |\psi_{1,\mathbf{k}}\rangle \langle \psi_{2,\mathbf{k}}| + \text{H.c.}$, $\tilde{s}_y = -i|\psi_{1,\mathbf{k}}\rangle \langle \psi_{2,\mathbf{k}}| + \text{H.c.}$, and $\tilde{s}_z = |\psi_{1,\mathbf{k}}\rangle \langle \psi_{1,\mathbf{k}}| - |\psi_{2,\mathbf{k}}\rangle \langle \psi_{2,\mathbf{k}}|$.

We can now integrate away the fermionic degrees of freedom and obtain a non-linear functional for the order

parameters

$$\mathcal{S} = \int_0^\beta d\tau \frac{1}{V} \text{Tr} [\hat{\Delta}^\dagger \hat{\Delta}] - \frac{1}{\beta} \text{Tr} \ln(-\mathcal{G}_0^{-1} + \Sigma), \quad (5)$$

with $-\mathcal{G}_0^{-1} = \partial_\tau + (H_0 - \mu)\tau_z$, $\Sigma = \tau_+ \hat{\Delta} + \tau_- \hat{\Delta}^\dagger$, $\beta = 1/T$ the inverse temperature, and the trace is over all the degrees of freedom, $\text{Tr} \equiv T \sum_\omega \int d\mathbf{k}$. As usual, the microscopic GL theory is obtained by expanding the non-linear action in powers of the fields,

$$\text{Tr} \ln(-\mathcal{G}_0^{-1} + \Sigma) = \text{Tr} \ln(-\mathcal{G}_0^{-1}) - \sum_{n=1}^{\infty} \frac{1}{n} \text{Tr} (\mathcal{G}_0 \Sigma)^n. \quad (6)$$

The forth order coefficient are determined by the forth order averages $\langle \Delta_{\mathbf{k}} \Delta_{\mathbf{k}}^* \Delta_{\mathbf{k}} \Delta_{\mathbf{k}}^* \rangle$, where $\langle \dots \rangle = T \sum_{\omega_n} \int \frac{d\mathbf{k}}{(2\pi)^3} G_+^2 G_-^2 \text{Tr}[\dots]$, $G_\pm = (i\omega_n \mp \xi_{\mathbf{k}})^{-1}$, $\xi_{\mathbf{k}} = \epsilon_{\mathbf{k}} - \mu$ and $\epsilon_{\mathbf{k}} = \sqrt{\mu^2 \tilde{\mathbf{k}}^2 + m^2}$ is the dispersion of the conduction band. Explicitly, the fourth order terms are given by

$$b_1 = 3\langle (\mathbf{d}_x \cdot \mathbf{d}_y)^2 \rangle + \langle (\mathbf{d}_x \times \mathbf{d}_y)^2 \rangle, \quad (7)$$

$$b_2 = -\langle (\mathbf{d}_x \cdot \mathbf{d}_y)^2 \rangle + \langle (\mathbf{d}_x \times \mathbf{d}_y)^2 \rangle. \quad (8)$$

Clearly, parallel vectors \mathbf{d}_i favor a chiral phase and orthogonal vectors favor a nematic phase.

IV. CHIRAL PHASE FOR STRONG ANISOTROPY

We now study the parameter b_2 as a function of the anisotropy of the system. By performing the averages one can approximate

$$b_2 = \frac{\kappa v^5}{v_z \mu^4 N_F} \int_0^\infty \frac{dkk}{2\pi} \int \frac{dk_z}{2\pi} \left[k_z^2 (k^2 + k_z^2) - \frac{k^4}{8} \right] \delta(\xi_{\mathbf{k}}), \quad (9)$$

where $\kappa = 7\zeta(3)N_F/(8(\pi T_c)^2)$ and $N_F = \int d^3\mathbf{k} \delta(\xi_{\mathbf{k}})/(2\pi)^3$ the density of states at the Fermi level. For an isotropic system the coefficient b_2 is positive and the nematic phase is favoured. By inspection of Eq. (9) it becomes clear how a strong anisotropy on the Fermi surface can drive the system into the $b_2 < 0$ regime.

The Hamiltonian Eq. (1) is linear in momentum and characteristic surface states of the TI arise when $\text{sign}(mv_z) < 0$ for states confined in $z < 0$ ⁴⁸. Nevertheless, quadratic terms in the mass term can be also considered and appear in more refined band structure calculations¹³

$$m(\mathbf{k}) = m - \alpha k^2 - \alpha_z k_z^2, \quad (10)$$

where $k^2 = k_x^2 + k_y^2$. For $m, \alpha, \alpha_z > 0$ the mass term changes sign on a particular surface in momentum space. This property yields a non-trivial topology of the insulator. For simplicity we neglect a spin- and orbital-independent term that adds to the Hamiltonian as a diagonal \mathbf{k} -dependent contribution that does not change the

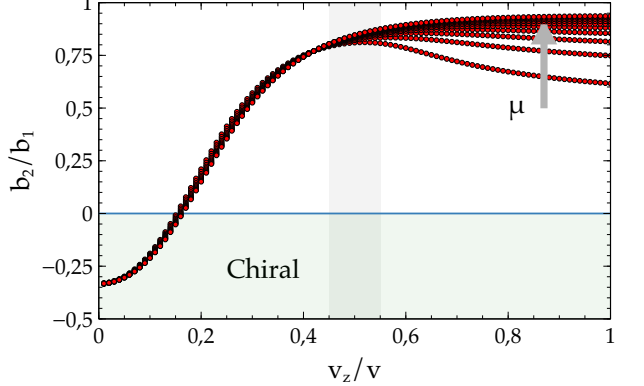


FIG. 1: (color online) Variation of the coefficient ratio b_2/b_1 as a function of the anisotropy of the system parametrized by v_z/v and the chemical potential μ , keeping the parameter α_z fixed. For sufficiently small v_z/v the coefficient b_2 becomes negative ($b_1 > 0$) and the chiral phase becomes possible.

topological properties of the system, a part from breaking the particle-hole symmetry of the Dirac Hamiltonian describing the topological insulator.

The momentum dependence of the mass term introduces a second scales α_z along the k_z direction, together with the velocity v_z , and consequently makes the Fermi surface intrinsically anisotropic. If α_z is neglected, the unique scale v_z can be reabsorbed in a redefinition of the momentum and it eventually factorize in the expression of b_1 and b_2 , in a way that their value become fixed and positive. It is then reasonable to study the parameter b_2 as we increase the anisotropy of the system.

The values of v_z and α_z can be controlled by chemical doping, in that dopants intercalates between the QL structure and modify the interlayer distance a_z and hopping t_z . The latter can be assumed to be exponentially dependent on a_z itself, $t_z = t_z^0 \exp(-a_z/R)$, with R a microscopic length scale characteristic of the p_z orbital of Se, and t_z^0 the amplitude of the hopping integral. It follows that an increase in the doping is expected to lower both v_z and α_z .

In Fig. 1 we plot the dependence of b_2/b_1 as a function of v_z/v , keeping α_z constant and taking for reference the parameters of the well known model of Ref. [13], $m = 0.28$ eV, $\alpha = 56.6$ eV Å², $\alpha_z = 10.0$ eV Å², and $v = 4.1$ eV Å. The coefficient α_z drops from the ratio. The shadowed regions indicate the region around $v_z = 2.2$ eV Å, that is realized in undoped material. We clearly see that by decreasing v_z/v we can obtain negative b_2 values. The strong topological character of the material allows a wide range of variation of v_z through doping, without changing the topological nature of the system, so that a chiral phase can be obtained by properly choosing the dopants and their amount.

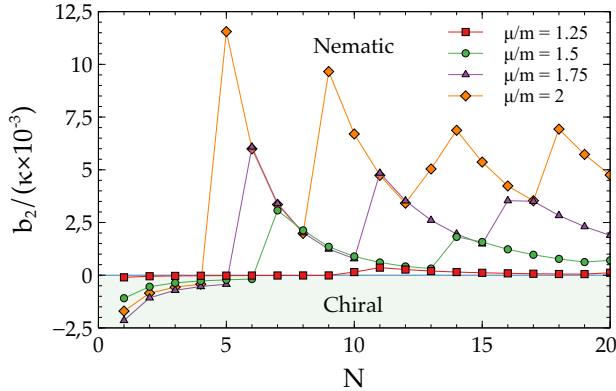


FIG. 2: (color online) Variation of the coefficient b_2 as a function of the number of layers N for different chemical potential. The parameter used in the tight-binding model are $t_0 = 0$, $t_1 = -4.1$ eV, $t_2 = 0.75$ eV, $t_z = -0.6$, $\lambda = 0.5$ eV, $a = 5.0$ Å, and $a_z = 9.1$ Å.

V. CHIRAL PHASE IN THIN SLABS

In 2D the Fermi surface is a line at $k_z = 0$, the coefficient b_2 Eq. (9) is negative, and the chiral phase is stable. The case $v_z \rightarrow 0$ and $\alpha_z \rightarrow 0$ is clearly realized when the system approaches the limit of quasi decoupled layers or the quasi 2D limit, characterized by an open Fermi surface⁴⁹. It is reasonable to study the stability of the nematic versus chiral phases for reduced thickness of the sample. In order to study the behaviour of the system by varying the number of QL layers we consider a simplified tight-binding model along the lines of Ref. [48].

We approximate the QL structure as a bilayer system composed by its top most (T) and bottom most (B) Se layers, described by triangular lattices on top of each other. The bilayer Hamiltonian is

$$H_{\text{TI}} = H_0 + H_R, \quad (11)$$

where H_0 describes spin-independent hopping within the same layer and nearest neighbor tunneling between the layers

$$\begin{aligned} H_0 = & t_0 \sum_{\langle i,j \rangle, \sigma} c_{i,\sigma,s}^\dagger c_{j,\sigma,s} + t_1 \sum_i c_{i,T,s}^\dagger c_{i,B,s} + \text{H.c.} \\ & + t_2 \sum_{\langle i,j \rangle, s} (c_{i,T,s}^\dagger c_{j,B,s} + c_{i,B,s}^\dagger c_{j,T,s}) \end{aligned} \quad (12)$$

with $\sigma = T, B$ labeling the two layers. Atoms in the two layers experience a local electric field along the $\pm \hat{z}$ direction that give rise to Rashba SOI of opposite sign on the two layer in the form

$$H_R = i\lambda \sum_{\langle ij \rangle, \sigma, ss'} p_\sigma c_{i,\sigma,s}^\dagger c_{j,\sigma,s'} \mathbf{s}_{ss'} \cdot \hat{z} \times \mathbf{a}_{ij}, \quad (13)$$

with $p_{T,B} = \pm 1$ and \mathbf{a}_{ij} a unit vector connecting site i and site j . The Hamiltonian H_{TI} describes a 2D TI,

whose small momentum expansion well approximates the Hamiltonian Eq. (10) with $m(\mathbf{k}) = 6t_2 + t_1 - 3t_2 a^2 (k_x^2 + k_y^2)/2$, $m = 6t_2 + t_1$, $\alpha = 3t_2 a^2/2$, and $v = 3\lambda a$. Along the z -direction the systems evolves with the Hamiltonian Eq. (14)

Along the z -direction the QL structure is repeated as a series of tightly bound QL planes weakly coupled by van der Waals forces. The entire structure along the z -direction realizes a Su Schrieffer Heeger (SSH) model⁵⁰,

$$H_{\text{SSH}} = \sum_j m_0 |T_j\rangle \langle B_j| + t_z |T_j\rangle \langle B_{j-1}| + \text{H.c.}, \quad (14)$$

with m_0 and t_z intracell and intercell hopping amplitudes. The SSH model is topologically non-trivial for $|t_z| > |m_0|$ and zero energy states localized at the boundary of the system appear as a signature of the non-trivial topology. In momentum space the Hamiltonian realizes a Dirac Hamiltonian around $k_z = 0$,

$$H_{\text{SSH}} = m\sigma_x + v_z k_z \sigma_y, \quad (15)$$

with $m = m_0 + t_z$. Momentum correction also arise at second order giving $m(k_z) = m - \alpha_z k_z^2$, $v_z = t_z a_z$, and $\alpha_z = t_z a_z^2/2$. A precise fitting of the band structure requires a much more detailed tight-binding model and it is beyond the scope of the present work. We then choose values of the tight-binding parameters t_0 , t_1 , t_2 , λ , and t_z , in a way that the band structure is well described by a Dirac equation at small momentum.

The coefficient b_2 is calculated with the Fourier transformed Hamiltonian $H(\mathbf{k}, n_z) = H_{\text{TI}}(\mathbf{k}) + H_{\text{SSH}}(\pi n_z / N a_z)$, where N is the number of layers, and by collecting the relevant terms in the fourth order expansion projected onto the conduction band

$$F_4 = \frac{\kappa}{N_F} \sum_{n_z, \mathbf{k}} \delta(\xi_{\mathbf{k}, n_z}) \text{Tr}[(\mathcal{P}_{\mathbf{k}, n_z} \Delta^\dagger \mathcal{P}_{\mathbf{k}, n_z} \Delta)^2], \quad (16)$$

where $\mathcal{P}_{\mathbf{k}, n_z} = \sum_{i=1,2} |\psi_{\mathbf{k}, i}\rangle \langle \psi_{\mathbf{k}, i}|$ is the projection operator of the conduction band subspace and $\Delta = -\psi_x \sigma_y s_y + \psi_y \sigma_y s_x$. We keep the tight-binding parameters fixed and only vary the number of layers N . In Fig. 2 we clearly see that the chiral phase is stable for sufficiently thin slabs of material. In particular, we see that the coefficient b_2 experiences quantum oscillations due to the coupling between the 2D layers. As a function of the chemical potential, small negative values of b_2 are obtained already for thick slabs and low doping, whereas larger negative b_2 values require higher doping and thinner slabs.

These results qualitatively show that a feasible way of obtaining a chiral phase could be through exfoliation and that the extreme case of a single layer is the best candidate for chiral superconductivity. The chiral solution is given by $\psi = \psi_0(1, i)$ so that the resulting gap on the Fermi surface reads

$$\Delta \propto \psi_0(k_y - ik_x) \tilde{s}_z. \quad (17)$$

This solution clearly applies to the single or few layer limit.

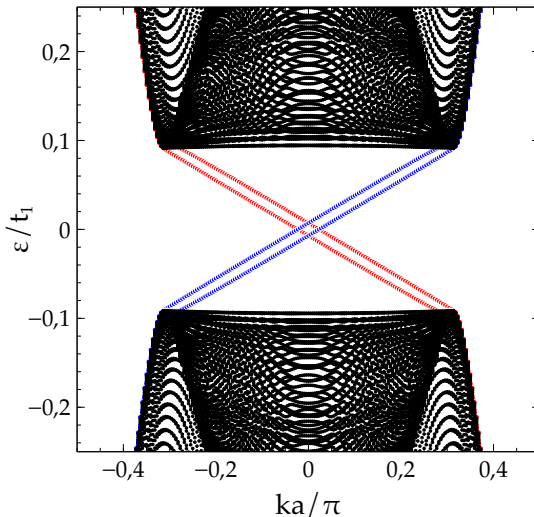


FIG. 3: Bands structure of a TI single layer with chiral superconductivity on a ribbon geometry. The parameters used are $t_0 = -0.1$, $t_1 = -5t_2$, $t_2 = 1.0$, $\lambda = 0.5$, $\Delta = 0.1$, and $\mu = 0.2$. Two Majorana edge states co-propagate on each side of the ribbon (blue on one side, red on the other side).

VI. CHIRAL MAJORANA MODES

We now discuss the topological character of the chiral phase focusing on the case of a single layer. In the 3D case the chiral phase of the E_u representation has been shown to produce Weyl nodes with topological charge $C = \pm 2$ on the north and south pole of the Fermi surface, respectively³². We then expect that in the 2D limit the topological charge gives rise to $C = 2$ co-propagating chiral Majorana modes on the edge of the system.

The BdG Hamiltonian Eq. (2) with the gap Eq. (17) projected onto the conduction band reads

$$H_{\text{BdG}} = \begin{pmatrix} \xi_{\mathbf{k}} & \Delta(k_x + ik_y)\tilde{s}_z \\ \Delta(k_x - ik_y)\tilde{s}_z & -\xi_{\mathbf{k}} \end{pmatrix}. \quad (18)$$

We see that both the spin up and spin down components are affected by a chiral $p_x + ip_y$ pairing, with gap of opposite sign for the two spin projections, due to the triplet nature of the pairing. Spinless chiral superconductivity in 2D opens a topologically non-trivial gap on the Fermi surface that gives rise to a single chiral Majorana mode at the boundary of the system, flowing with a velocity $v_M = \mp|\Delta|/k_F$, for the $p_x \pm ip_y$ cases, respectively. We then expect two chiral Majorana modes that co-propagate at the boundary of the system with $v_M = -|\Delta|/k_F$, with Δ the mean-field value of the order parameter ψ_0 in Eq. (17).

The mean-field Hamiltonian is $H_{\text{MF}} = H + H_{\text{sc}}$, with H_{sc} the Hamiltonian term describing superconductivity at mean field level in the chiral phase

$$H_{\text{sc}} = \sum_{i;\sigma s,\sigma' s'} c_{i,\sigma s}^\dagger c_{i,\sigma' s'}^\dagger \hat{\Delta}_{\sigma s;\sigma' s'} + \text{H.c.}, \quad (19)$$

with $\hat{\Delta} = \Delta \sigma_y (s_x + is_y) is_y$. The band structure on a ribbon geometry is shown in Fig. 3, where clear co-propagating chiral Majorana modes appear, blue on one side and red on the other side, thus confirming the prediction based on the topological charge and the small momentum expansion.

VII. CONCLUSION

In this work we studied the stability of the chiral phase versus the nematic phase in Bi_2Se_3 as a function of the anisotropy of the system and the thickness of the sample. We showed that in strongly anisotropic systems and in thin slabs the chiral phase is favoured, giving rise to a chiral topological superconductor that hosts two co-propagating chiral Majorana modes at its boundary. Our findings show that upon engineering strongly anisotropic conditions or by exfoliation down to $N < 10$ layer thin films the chiral phase is allowed, opening the route to topological quantum computations with Majorana modes.

VIII. ACKNOWLEDGMENTS

The author acknowledges useful discussion with F. Finocchiaro, F. de Juan, and F. Guinea. This work is supported by the European Union's Seventh Framework Programme (FP7/2007-2013) through the ERC Advanced Grant NOVGRAPHENE (GA No. 290846) and the Comunidad de Madrid through the grant MAD2DCM, S2013/MIT-3007.

* Electronic address: luca.chiroli@imdea.org

¹ M. Sigrist and K. Ueda, Rev. Mod. Phys. **63**, 239 (1991).

² X.-L. Qi and S.-C. Zhang, Rev. Mod. Phys. **83**, 1057 (2011).

³ N. Read and D. Green, Phys. Rev. B **61**, 10267 (2000).

⁴ D. A. Ivanov, Phys. Rev. Lett. **86**, 268 (2001).

⁵ J. Alicea, Reports on Progress in Physics **75**, 076501

(2012).

⁶ C. W. J. Beenakker, Annual Review of Condensed Matter Physics **4**, 113 (2013).

⁷ R. Aguado, ArXiv e-prints (2017), 1711.00011.

⁸ T. Meng and L. Balents, Phys. Rev. B **86**, 054504 (2012).

⁹ J. D. Sau and S. Tewari, Phys. Rev. B **86**, 104509 (2012).

¹⁰ S. A. Yang, H. Pan, and F. Zhang, Phys. Rev. Lett. **113**,

046401 (2014).

¹¹ C. Nayak, S. H. Simon, A. Stern, M. Freedman, and S. Das Sarma, *Rev. Mod. Phys.* **80**, 1083 (2008).

¹² S. D. Sarma, M. Freedman, and C. Nayak, *Npj Quantum Information* **1**, 15001 (2015).

¹³ H. Zhang, C.-X. Liu, X.-L. Qi, X. Dai, Z. Fang, and S.-C. Zhang, *Nature Physics* **5**, 438 (2009).

¹⁴ M. Z. Hasan and C. L. Kane, *Rev. Mod. Phys.* **82**, 3045 (2010).

¹⁵ L. Fu and E. Berg, *Phys. Rev. Lett.* **105**, 097001 (2010).

¹⁶ Y. S. Hor, A. J. Williams, J. G. Checkelsky, P. Roushan, J. Seo, Q. Xu, H. W. Zandbergen, A. Yazdani, N. P. Ong, and R. J. Cava, *Phys. Rev. Lett.* **104**, 057001 (2010).

¹⁷ L. A. Wray, S.-Y. Xu, Y. Xia, Y. S. Hor, D. Qian, A. V. Fedorov, H. Lin, A. Bansil, R. J. Cava, and M. Z. Hasan, *Nature Physics* **6**, 855 (2010).

¹⁸ M. Kriener, K. Segawa, Z. Ren, S. Sasaki, and Y. Ando, *Phys. Rev. Lett.* **106**, 127004 (2011).

¹⁹ S. Sasaki, M. Kriener, K. Segawa, K. Yada, Y. Tanaka, M. Sato, and Y. Ando, *Phys. Rev. Lett.* **107**, 217001 (2011).

²⁰ N. Levy, T. Zhang, J. Ha, F. Sharifi, A. A. Talin, Y. Kuk, and J. A. Stroscio, *Phys. Rev. Lett.* **110**, 117001 (2013).

²¹ H. Peng, D. De, B. Lv, F. Wei, and C.-W. Chu, *Phys. Rev. B* **88**, 024515 (2013).

²² Shruti, V. K. Maurya, P. Neha, P. Srivastava, and S. Pattnaik, *Phys. Rev. B* **92**, 020506 (2015).

²³ Z. Liu, X. Yao, J. Shao, M. Zuo, L. Pi, S. Tan, C. Zhang, and Y. Zhang, *Journal of the American Chemical Society* **137**, 10512 (2015).

²⁴ Z. Wang, A. A. Taskin, T. Frölich, M. Braden, and Y. Ando, *Chemistry of Materials* **28**, 779 (2016).

²⁵ T. Asaba, B. J. Lawson, C. Tinsman, L. Chen, P. Corbae, G. Li, Y. Qiu, Y. S. Hor, L. Fu, and L. Li, *Phys. Rev. X* **7**, 011009 (2017).

²⁶ K. Matano, M. Kriener, K. Segawa, Y. Ando, and G.-q. Zheng, *Nature Physics* **12**, 852 EP (2016).

²⁷ S. Yonezawa, K. Tajiri, S. Nakata, Y. Nagai, Z. Wang, K. Segawa, Y. Ando, and Y. Maeno, *Nature Physics* **13**, 123 EP (2016).

²⁸ Y. Pan, A. M. Nikitin, G. K. Araizi, Y. K. Huang, Y. Matsushita, T. Naka, and A. de Visser, *Scientific Reports* **6**, 28632 EP (2016).

²⁹ M. P. Smylie, H. Claus, U. Welp, W.-K. Kwok, Y. Qiu, Y. S. Hor, and A. Smezhko, *Phys. Rev. B* **94**, 180510 (2016).

³⁰ J. Shen, W.-Y. He, N. F. Q. Yuan, Z. Huang, C.-w. Cho, S. H. Lee, Y. S. Hor, K. T. Law, and R. Lortz, *npj Quantum Materials* **2**, 59 (2017).

³¹ L. Fu, *Phys. Rev. B* **90**, 100509 (2014).

³² J. W. F. Venderbos, V. Kozii, and L. Fu, *Phys. Rev. B* **94**, 180504 (2016).

³³ T. Hashimoto, K. Yada, A. Yamakage, M. Sato, and Y. Tanaka, *Journal of the Physical Society of Japan* **82**, 044704 (2013).

³⁴ Y. Nagai and Y. Ota, *Phys. Rev. B* **94**, 134516 (2016).

³⁵ J. W. F. Venderbos, V. Kozii, and L. Fu, *Phys. Rev. B* **94**, 094522 (2016).

³⁶ S. A. Yang, H. Pan, and F. Zhang, *Phys. Rev. Lett.* **113**, 046401 (2014).

³⁷ F. Wu and I. Martin, *Phys. Rev. B* **95**, 224503 (2017).

³⁸ A. A. Zyuzin, J. Garaud, and E. Babaev, *Phys. Rev. Lett.* **119**, 167001 (2017).

³⁹ L. Chiroli, F. de Juan, and F. Guinea, *Phys. Rev. B* **95**, 201110 (2017).

⁴⁰ N. F. Q. Yuan, W.-Y. He, and K. T. Law, *Phys. Rev. B* **95**, 201109 (2017).

⁴¹ F. Wu and I. Martin, *Phys. Rev. B* **96**, 144504 (2017).

⁴² M. Hecker and J. Schmalian, *ArXiv e-prints* (2017), 1712.07523.

⁴³ Y. Zhang, K. He, C.-Z. Chang, C.-L. Song, L.-L. Wang, X. Chen, J.-F. Jia, Z. Fang, X. Dai, W.-Y. Shan, et al., *Nature Physics* **6**, 712 EP (2010).

⁴⁴ G. Zhang, H. Qin, J. Chen, X. He, L. Lu, Y. Li, and K. Wu, *Advanced Functional Materials* **21**, 2351 (2011).

⁴⁵ S. Nakosai, Y. Tanaka, and N. Nagaosa, *Phys. Rev. Lett.* **108**, 147003 (2012).

⁴⁶ L. Chiroli, J. P. Baltanás, and D. Frustaglia, *ArXiv e-prints* (2018), 1801.01736.

⁴⁷ L. Fu, *Phys. Rev. Lett.* **115**, 026401 (2015).

⁴⁸ T. H. Hsieh and L. Fu, *Phys. Rev. Lett.* **108**, 107005 (2012).

⁴⁹ E. Lahoud, E. Maniv, M. S. Petrushevsky, M. Naamneh, A. Ribak, S. Wiedmann, L. Petaccia, Z. Salman, K. B. Chashka, Y. Dagan, et al., *Phys. Rev. B* **88**, 195107 (2013).

⁵⁰ W. P. Su, J. R. Schrieffer, and A. J. Heeger, *Phys. Rev. Lett.* **42**, 1698 (1979).